Quaternary $Rb_2Cu_2SnS_4$, $A_2Cu_2Sn_2S_6$ (A = Na, K, Rb, Cs), $A_2Cu_2Sn_2Se_6$ (A = K, Rb), $K_2Au_2SnS_4$, and $K_2Au_2Sn_2S_6$. Syntheses, Structures, and Properties of New Solid-State Chalcogenides Based on Tetrahedral $[SnS_4]^{4-}$ Units

Ju-Hsiou Liao and Mercouri G. Kanatzidis*

Department of Chemistry and Center for Fundamental Materials Research, Michigan State University, East Lansing, Michigan 48824

Received April 2, 1993. Revised Manuscript Received August 16, 1993®

$Rb_2Cu_2SnS_4$ (**I**) and $Rb_2Cu_2Sn_2S_6$ (**II**) were synthesized by heating a mixture of Sn, Cu, Rb_2S, and S in the ratios of 1:4:4:16 and 1:1–2:4:16, respectively, at 400 °C for 4 days. $K_2Au_2SnS_4$ (**III**) and $K_2Au_2Sn_2S_6$ (**IV**) were synthesized by heating mixtures of Sn, Au, K_2S, and S in the ratios of 1:2:4:16 and 1:1.5:2:16, respectively, at 350 °C for 4 days. The structures were characterized by single-crystal X-ray diffraction techniques, infrared spectroscopy and UV–vis–near-IR reflectance spectroscopy. Crystal data for **I**: space group *Ibam* (No. 72); a = 5.528(4) Å, b = 11.418(6) Å, c = 13.700(6) Å; Z = 4; V = 865(2) Å^3; d_{calc} = 4.185 g/cm^3; number of data collected 468; number of data observed ($I > 3\sigma(I)$) 221; number of variables 23; final R/R_W = 6.9/8.1. Crystal data for **II**: space group $C2/c$ (No. 15); a = 11.026(2) Å, b = 11.019(3) Å, c = 20.299(4) Å, β = 97.79(2)°; Z = 8; V = 2444(1) Å^3; d_{calc} = 3.956 g/cm^3; number of data collected 11 691; number of data observed ($I > 3\sigma(I)$) 1756; number of variables 111; final R/R_W = 6.3/6.4. Crystal data for **III**: space group $P\bar{1}$ (No. 2); a = 8.212(4) Å, b = 9.110(4) Å, c = 7.314(2) Å, α = 97.82(3)°, β = 111.72(2)°, γ = 72.00(2)°, V = 483.2(7) Å^3; Z = 2; d_{calc} = 4.941 g/cm^3; number of data collected: 1832; number of data observed ($I > 3\sigma(I)$) 1447; number of variables 83; final R/R_W = 4.8/6.0. Crystal data for **IV**: space group $P4/mcc$ (No. 124); $a = b$ = 7.968(2) Å, c = 19.200(6) Å, V = 1219(1) Å^3, Z = 4; d_{calc} = 4.914 g/cm^3; number of data collected 911; number of data observed ($I > 3\sigma(I)$) 459; number of variables 34; final R/R_W = 4.1/3.9. **I** has a two-dimensional structure which contains CuS_4 and SnS_4 tetrahedra in the ratio of 2:1 as building blocks. The $[Cu_2SnS_4]^{2-}$ layers are best described as an ordered defect anti-PbO type structure. The rubidium cations are found between the layers. **II** is a layered structure which contains corner-sharing SnS_4 and CuS_4 tetrahedra and can be viewed as a derivative of adamantine type structure. Both **III** and **IV** have one-dimensional structures. The anionic chains of **III** contain linear AuS_2 and SnS_4 tetrahedra in the ratio of 2:1, while **IV** contains linear AuS_2 and Sn_2S_6 edge-sharing bitetrahedra also in the ratio of 2:1. The charges are balanced by potassium cations located between the chains. Infrared spectra for **I**–**IV** are reported. **I**–**IV** are semiconductors with optical bandgaps of 2.08, 1.44, 2.75, and 2.30 eV, respectively.

Introduction

Chalcogenides of the transition and main-group metals exhibit useful physical and chemical properties which are promising for applications in nonlinear optics,[1] rechargeable battery cathodes,[2] optical storage,[3] radiation detection,[4] solar energy conversion,[5] and catalysts.[6] Binary and ternary chalcogenides have been extensively investigated, but relatively little is known about quaternary chalcogenides which may also exhibit interesting properties. Tetrathiometalates, especially $[MoS_4]^{2-}$ and $[WS_4]^{2-}$, have been extensively used as building blocks to synthesize heterometallic discrete molecular sulfido complexes by self-assembly reactions in solution.[7] A few examples of solid state have been reported. One interesting example is the formation of $(NH_4)CuMoS_4$[8] which contains linear

* Abstract published in *Advance ACS Abstracts*, October 1, 1993.

(1) (a) Finlayson, N.; Banyai, W. C.; Seaton, C. T.; Stegeman, G. I.; O'Neil, M.; Cullen, T. J.; Ironside, G. N. *J. Opt. Soc. Am.* **1989**, *6B*, 675–684. (b) Wang, Y.; Herron, N.; Mahler, W.; Suna, A. *J. Opt. Soc. Am.* **1989**, *6B*, 808–813. (c) Ballman, A. A.; Byer, R. L.; Eimerl, D.; Feigelson, R. S.; Feldman, B. J.; Goldberg, L. S.; Menyuk, N.; Tang, C. L. *Appl. Opt.* **1987**, *26*, 224–227.

(2) (a) Whittingham, M. S. *Prog. Solid State Chem.* **1978**, *12*, 41–99. (b) Whittingham, M. S. In *Solid State Ionic Devices*, July 18–23, 1988, Singapore; Chowdari, B. V. R., Radhakrishna, S., Eds.; World Scientific: Singapore, 1988; pp 55–74. (c) Bowden, W. L.; Barnette, L. H.; DeMuth, D. L. *J. Electrochem. Soc.* **1989**, *136*, 1614–1618. (d) Murphy, D. W.; Trumbore, F. A. *J. Electrochem. Soc.* **1987**, *134*, 2506–2507. (e) Whittingham, M. S. *Science* **1976**, *192*, 1125. (f) Whittingham, M. S. *J. Solid State Chem.* **1979**, *29*, 303–310.

(3) (a) Eckert, H. *Angew Chem., Int. Ed. Engl., Adv. Mater.* **1989**, *28*, 1723–1732. (b) Zallen, R. In *Physics of Amorphous Solids*; Wiley: New York, 1983. (c) Strand, D.; Adler, D. *Proc. SPIE Int. Soc. Opt. Eng.* **1983**, *420*, 200. (d) Yamada, N.; Ohno, N.; Akahira, N.; Nishiuchi, K.; Nagata, K.; Takao, M. *Proc. Int. Symp. Optical Memory, 1987, Jpn. J. Appl. Phys.* **1987**, *26*, Suppl. 26–4, p 61. (e) Arnautova, E.; Sviridov, E.; Rogach, E.; Savchenko, E.; Grekov, A. *Intergr. Ferroelectr.* **1992**, *1*, 147–150.

(4) (a) Smith, R. A. In *Semiconductors*; Cambridge University Press: Cambridge, 1978; p 438. (b) Bartlett, B. E.; et al. *Infrared Phys.* **1969**, *9*, 35.

(5) (a) Mickelsen, R. A.; Chen, W. S. In *Ternary and Multinary Compounds*; Proceedings of the 7th Conference; Deb, S. K., Zunger, A., Eds.; Materials Research Society: Pittsburgh, 1987; pp 39–47. (b) Steward, J. M., Chen, W. S., Devaney, W. E., Mickelsen, R. A., Deb, S. K., Zunger, A., Eds.; Materials Research Society: Pittsburgh, 1987; pp 59–64.

(6) (a) Chianelli, R. R.; Pecoraro, T. A.; Halber, T. R.; Pan, W.-H.; Stiefel, E. I. *J. Catal.* **1984**, *86*, 226–230. (b) Pecoraro, T. A.; Chianelli, R. R. *J. Catal.* **1981**, *67*, 430–445. (c) Harris, S.; Chianelli, R. R. *J. Catal.* **1984**, *86*, 400–412.

(7) (a) Coucouvanis, D. *Acc. Chem. Res.* **1981**, *14*, 201–209. (b) Holm, R. H. *Chem. Soc. Rev.* **1981**, *10*, 455–491. (c) Müller, A.; Diemann, E.; Jostes, R.; Bögge, H. *Angew. Chem., Int. Ed. Engl.* **1981**, *20*, 934–955.

0897-4756/93/2805-1561$04.00/0

chains composed of $[MoS_4]^{2-}$ tetrahedra chelated to Cu^+ ions. Recently, a two-dimensional heterometallic sulfide, Cu_2WS_4, was reported to form in powder form by mixing $[WS_4]^{2-}$ and Cu^+ in DMF solution.[9] Although these tetrahedral anions work well as ligands in solution they are thermally unstable and cannot be used at higher temperature. Other tetrathiometalates, however, are considerably more stable (e.g., $[SnS_4]^{4-}$, $[GeS_4]^{4-}$, $[PS_4]^{3-}$) and their coordination properties toward other metal ions to form solid-state lattices are worthy of investigation. During our studies of ternary alkali-metal-containing tin (poly)sulfides using reactive molten salts as solvents, we noticed that $[SnS_4]^{4-}$ and $[Sn_2S_6]^{4-}$ ions are the basic units comprising various anionic frameworks and can actually be isolated, as their alkali-metal salts by either increasing the reaction temperatures or adding more A_2S (A = alkali metal) in the polysulfide fluxes.[10a] These anions are well known since 1971.[10g-j] If then $[SnS_4]^{4-}$ and/or $[Sn_2S_6]^{4-}$ exists or is generated in Sn-containing polysulfide melts, they could be used in reactions with other metal ions to form new heterometallic sulfides. Some examples showing the presence of tetrahedral $[SnS_4]^{4-}$ fragments in solid-state quaternary chalcogenides synthesized at high temperatures have been reported.[11,12] They include $BaAg_2SnS_4$, $BaAu_2SnS_4$, $BaCu_2SnS_4$, $SrCu_2SnS_4$, $BaHgSnS_4$, $BaCdSnS_4$, $KGaSnS_4$, and $Cu_2B^{II}SnS_4$ (B^{II} = Mn, Fe, Co, Ni, Zn, Cd, or Hg). Here we attempted to exploit three properties associated with Sn-containing polysulfide fluxes: (a) the relatively low temperature accessible for synthesis, $T < 500$ °C; (b) the apparent ability of these fluxes to supply the $[SnS_4]^{4-}$ anion for reaction chemistry; (c) the anticipated excellent coordinating ability of the $[SnS_4]^{4-}$ anion toward transition metals in a similar fashion observed for the $[MoS_4]^{2-}$ unit.[7] If the metals, to coordinate to $[SnS_4]^{4-}$, are chosen to prefer tetrahedral coordination, the products are expected to be based on tetrahedral substructures. Examples of such metals would be Cu^+, Zn^{2+}, and Cd^{2+}, etc. Indeed, quaternary chalcogenides of the $Cu_2B^{II}SnS_4$ type (B^{II} = Mn, Fe, Co, Ni, Zn, Cd, or Hg)[12b] adopt structures derived from simple sphalerites or wurtzites. If, on the other hand, metals with other coordination preferences are chosen, such as Au^+ (linear) or Pt^{2+} (square planar), a departure from the overall tetrahedral motif is expected. Using Cu^+ and Au^+, we explored the partial charge "neutralization" of the $[SnS_4]^{4-}$ anion in A_2S_x (A = alkali metal) flux as the reaction medium. To avoid possible anticipated crystallographic difficulties in distinguishing Sn from Ag the latter element was not chosen for this investigation. Here we report on several new quaternary compounds: $Rb_2Cu_2SnS_4$, $A_2Cu_2Sn_2S_6$ (A = Na, K, Rb, Cs), $A_2Cu_2Sn_2Se_6$ (A = K, Rb), $K_2Au_2SnS_4$, and $K_2Au_2Sn_2S_6$ obtained from the above methodology.

Experimental Section

All work was done under a nitrogen atmosphere. Reagents: Sn metal, ~325 mesh, 99.8% purity, CERAC Inc., Milwaukee, WI. Cu metal, electronic dust, purified, Fisher, Scientific Co., Fair Lawn, NJ. Au metal, ~325 mesh, 99.95% purity, CERAC Inc., Milwaukee, WI. Sublimed sulfur was purchased from J. T. Baker Chemical Co. 99.5–100.5%. K_2S and Rb_2S starting materials were prepared as described elsewhere.[13] All reagents were stored under N_2 in a glovebox. The X-ray powder diffraction patterns were recorded with a Phillips XRD-3000 diffractometer controlled by a PDP 11 computer and operating at 40 kV/20 mA. Ni-filtered Cu radiation was used. Quantitative microprobe analyses were performed on a JEOL 35CF scanning electron microscope (SEM) equipped with Tracor Northern TN5500 X-ray microanalysis. The standardless quantitative (SQ) analysis program uses multiple least-square analysis and a ZAF matrix correction procedure to calculate elemental concentrations. Known compounds containing the elements of interest were used for calibration. IR spectra were recorded as CsI pellets with a Nicolet 740 Fourier transform infrared spectrometer in 4-cm^{-1} resolution. Optical diffuse reflectance spectra were measured at room temperature with a Shimadzu UV-3101PC double-beam, double-monochromator spectrophotometer. The sample was ground into powder and pressed into a thin layer above $BaSO_4$ on a sample holder. $BaSO_4$ powder was used as reference. The absorption spectrum was calculated from the reflectance data using the Kubelka–Munk function:[14] $\alpha/S = (1-R)^2/2R$. R is the reflectance, α is the absorption coefficient, and S is the scattering coefficient which is practically wavelength independent when the particle size is larger than 5 μm.

Synthesis. *$Rb_2Cu_2SnS_4$ (I)*: A mixture of Sn powder (0.039 g, 0.33 mmol), Cu powder (0.084 g, 1.32 mmol), Rb_2S (0.267 g, 1.32 mmol), and S (0.171 g, 5.28 mmol) in the ratio of 1:4:4:16 was loaded into a ~5-mL Pyrex tube in a N_2 glovebox. The tube was evacuated and sealed at a pressure of $\sim 10^{-3}$ Torr. The mixture was heated slowly from room temperature to 400 °C in 12 h in a furnace programmed by a personal computer. The temperature was kept at 400 °C for 4 days, and then was cooled slowly to room temperature at 4 °C/h. Orange platelike crystals were formed in ~71% yield (based on Sn). The product was washed with degassed DMF to remove excess Rb_2S_x flux using a standard Schlenk technique and was dried with acetone and ether. The orange crystals are insoluble in water and common organic solvents but decompose slowly in air. Semiquantitative elemental analyses performed on a scanning electron microscope (SEM) using an energy-dispersive (EDS) microscopic technique indicated $Rb_{2.2}Cu_{3.4}Sn_{1.0}S_{4.2}$. IR: 353 cm^{-1} with a shoulder at 329 cm^{-1}.

$Rb_2Cu_2Sn_2S_6$ (II): The procedure for preparation and isolation of **II** is the same as described above except that molar ratios of 1:1–2:4:16 (Sn:Cu:Rb_2S:S) were used. Black crystals of **II** were obtained in 62% yield (based on Sn). These crystals exhibit mica-like thin-layered morphology and are easily separated into very thin sheets. They are stable in air and insoluble in water and common organic solvents. Semiquantitative elemental analysis performed on SEM/EDS indicated $Rb_{1.0}Cu_{1.5}Sn_{1.0}S_{3.1}$. IR: 392 (s), 369 (m), 349 (m), 305 (m), 264 (s), 232 (s), 198 (m) cm^{-1}.

Other X-ray isomorphous $A_2Cu_2Sn_2Q_6$ (A = Na, K, Rb, Cs: Q = S, Se) phases prepared by a similar procedure are (a) K_2Cu_2-

(8) Binnie, W. P.; Redman, M. J.; Mallio, W. *Inorg. Chem.* **1970**, *9*, 1449–1452.

(9) Pruss, E. A.; Snyder, B. S.; Stacy, A. M. *Angew. Chem. Int. Ed. Engl.* **1993**, *32*, 256–257.

(10) (a) Liao, J.-H.; Varotsis, C.; Kanatzidis, M. G. *Inorg. Chem.* **1993**, *32*, 2453–2462. (b) Krebs, B.; Schiwy, W. *Z. Anorg. Chem.* **1973**, *393*, 63–71. (c) Schiwy, W.; Blutau, Chr.; Gathje, D.; Krebs, B. *Z. Anorg. Allg. Chem.* **1975**, *412*, 1–10. (d) Jumas, J.-C.; Philippot, E.; Maurin, M. *J. Solid State Chem.* **1975**, *14*, 152–159. (e) Mark, W.; Lindqvist, O.; Jumas, J.-C.; Philippot, E. *Acta. Crystallogr.* **1974**, *B30*, 2620–2628. (f) Sheldrick, W. S. *Z. Anorg. Allg. Chem.* **1988**, *562*, 23–30. (g) Krebs, B.; Pohl, S.; Schiwy, W. *Z. Anorg. Chem.* **1972**, *393*, 241–252. (h) Jumas, J.-C.; Philippot, E.; Vermot-Gaud-Daniel, F.; Ribes, M.; Maurin, M. *J. Solid State Chem.* **1975**, *14*, 319–327. (i) Schiwy, W.; Pohl, S.; Krebs, B. *Z. Anorg. Allg. Chem.* **1973**, *402*, 77–86. (j) Susa, K.; Steinfink, H. *J. Solid State Chem.* **1971**. *3*, 75–82.

(11) (a) Teske, Chr. L. *Z. Anorg. Allg. Chem.* **1978**, *445*, 193–201. (b) Teske, Chr. L.; Vetter, O. *Z. Anorg. Allg. Chem.* **1976**, *427*, 200–204. (c) Teske, Chr. L. *Z. Naturforsch* **1980**, *35b*, 7–11. (d) Teske, Chr. L. *Z. Anorg. Allg. Chem.* **1976**, *419*, 67–76. (e) Teske, Chr. L.; Vetter, O. *Z. Anorg. Allg. Chem.* **1976**, *426*, 281–287. (f) Teske, Chr. L. *Z. Anorg. Allg. Chem.* **1980**, *460*, 163–168.

(12) (a) Wu, P.; Lu, Y.-J.; Ibers, J. A. *J. Solid Chem.* **1992**, *97*, 383–390. (b) Guen, L.; Glaunsinger, W. S. *J. Solid State Chem.* **1980**, *35*, 10–21.

(13) Klemm, W.; Sodomann, H.; Langmesser, P. *Z. Anorg. Allg. Chem.* **1939**, *241*, 281–304.

(14) (a) Kubelka, P.; Munk, F. *Z. Tech. Phys.* **1931**, *12*, 539. (b) Kubelka, P. *J. Opt. Soc. Am.* **1948**, *38*, 448. (c) Wendlandt, W. W.; Hecht, H. G. *Reflectance Spectroscopy*; Interscience Publishers: New York, 1966. (d) Kotüm, G. *Reflectance Spectroscopy*; Springer Verlag, New York, 1969. (e) Tandon, S. P.; Gupta, J. P. *Phys. Status Solidi* **1970**, *38*, 363–367.

Table I. Summary of Crystallographic Data for $Rb_2Cu_2SnS_4$, $Rb_2Cu_2Sn_2S_6$, $K_2Au2SnS_4$, and $K_2Au_2Sn_2S_6$[a]

	I	II	III	IV
formula	$Rb_2Cu_2SnS_4$	$Rb_2Cu_2Sn_2S_6$	$K_2Au_2SnS_4$	$K_2Au_2Sn_2S_6$
fw	544.96	727.77	719.06	901.87
a, Å	5.528(4)	11.026(2)	8.212(4)	7.968(2)
b, Å	11.418(6)	11.019(3)	9.110(4)	7.968(2)
c, Å	13.700(6)	20.299(4)	7.314(2)	19.200(6)
α	90.0	90.0	97.82(3)	90.0
β	90.0	97.79(2)	111.72(2)	90.0
γ	90.0	90.0	72.00(3)	90.0
Z, V, Å^3	4, 865(2)	8, 2441(1)	2, 483.2(7)	4, 1219(1)
space group	*Ibam*	*C*2/*c*	$P\bar{1}$	*P*4/*mcc*
d_{calc}, g/cm3	4.185	3.956	4.941	4.914
crystal size, mm	0.30 × 0.40 × 0.04	0.82 × 0.73 × 0.31	0.40 × 0.54 × 0.53	0.20 × 0.20 × 0.33
radiation	Mo Kα	Mo Kα	Mo Kα	Mo Kα
μ(Mo Kα), cm^{-1}	195.02	161.51	343.92	296.20
$2\theta_{max}$, deg	50.0	60	50.0	55.0
no. of data collected	468	11691	1832	911
no. of unique data	468	3736	1700	911
no. of observed data ($I > 3.0\sigma(I)$)	221	1756	1447	459
no. of variables	23	23	83	34
final R/R_w, %	6.9/8.1	6.3/6.4	4.8/6.0	4.1/3.9

[a] At 23 °C. $R = \sum||F_o| - |F_c||/\sum|F_o|$. $R_w = \{\sum w(|F_o| - |F_c|)^2/\sum w|F_o|^2\}^{1/2}$.

Sn_2S_6, (b) $K_2Cu_2Sn_2Se_6$, (c) $Rb_2Cu_2Sn_2Se_6$, (d) $Na_2Cu_2Sn_2S_6$, and (e) $Cs_2Cu_2Sn_2S_6$. All of them are black and exhibit thin-layer morphology. The reactions for a–c gave good yields (>70%). K^+ and Rb^+ seem to be preferred for the formation of $A_2Cu_2Sn_2Q_6$ phases. (d) and (e) gave low yield and were present with other binary and ternary products.

$K_2Au_2SnS_4$ (III): A mixture of Sn (0.015 g, 0.13 mmol), Au (0.050 g, 0.25 mmol), K_2S (0.055 g, 0.50 mmol), and S (0.064 g, 2.0 mmol) in a ratio of 1:2:4:16 was loaded into a ~5-mL Pyrex tube in a dry N_2 glovebox. The tube was evacuated and flame sealed at a pressure of ~10^{-3} Torr. The mixture was heated slowly from room temperature to 350 °C in 12 h in a furnace programmed by a personal computer. The temperature was kept at 350 °C for 4 days and then was cooled slowly to room temperature at 4 °C/h. Yellow long parallelepiped crystals of **II** were obtained by removing the excess K_2S_x flux with degassed DMF under N_2 atmosphere. The final product was washed and dried with acetone and ether. Yield: 66% (based on Sn). The yellow crystals are stable in air but break apart into fibers in water and dissolve slowly to form a light yellow solution. The crystals show a fibrous feature when crushed and are hard to grind. SEM/EDS indicated $K_{1.1}Au_{1.5}Sn_{1.0}S_{3.4}$. IR: 509 (w), 368 (m), 347 (m), 339 (s), 328 (m), and 153 cm^{-1} (w).

$K_2Au_2Sn_2S_6$ (IV): The procedure for preparation and isolation was the same as that of **III** except that a molar ratio of 1:1.5:2:16 (Sn:Au:K_2S:S) was used. Orange chunky crystals were obtained in 53% yield (based on Sn). The crystals are stable in air and insoluble in water and common organic solvents. They also split into fibers when crushed and are very hard to grind into fine powder. Semiquantitative elemental analysis performed on SEM/EDS indicated $K_{0.9}Au_{1.2}Sn_{1.0}S_{4.0}$. IR: 359 (s), 337 (s), 320 (s), 311 (m), 298 (s), 189 (m), 178 (w), 171 (w), 158 (m), and 151 cm^{-1} (m).

X-ray Diffraction Analysis. The homogeneity of **I–IV** compounds was confirmed by comparing the experimental powder X-ray diffraction patterns to their theoretical patterns[15] calculated using the cell parameters and atomic coordinates obtained from single-crystal X-ray diffraction analyses.

The single crystal X-ray diffraction data of **I–IV** were collected on a Rigaku AFC6S four-circle diffractometer suing ω–2θ scan mode. Graphite-monochromated Mo Kα radiation was used and all data sets were collected at room temperature. The crystals were mounted at the end of glass fibers. The stability of the experimental setup and crystal integrity were monitored by measuring three standard reflections periodically every 150 reflections. No significant decay was observed during the data collections. **II** tends to grow twinned crystals. A large number of crystals had to be screened before a satisfactory single crystal was found. To obtain better refinement, Friedel pairs of **II** were collected and the data were averaged. The structures were solved with direct methods (SHELXS-86)[16] and were refined by a full-matrix least-square technique available in the TEXSAN[17] programs running on a VAXstation 3100/76 computer. An empirical absorption correction was applied to all the data (based on ψ scans). An additional absorption correction following the DIFABS[18] procedure was applied to isotropically refined data.

The crystallographic data and detailed information of structure solution and refinement for **I–IV** are listed in Table I. Atomic coordinates and equivalent isotropic thermal parameters are given in Tables II–V, respectively.

Table II. Positional Parameters and Equivalent Isotropic Displacement Values (Å^2)[a] for $Rb_2Cu_2SnS_4$ with Estimated Standard Deviations in Parentheses

atom	x	y	z	B(eq)
Sn	0	0	0.25	1.5(2)
Rb	0.2725(7)	0.1252(4)	0.5	2.2(2)
Cu	0	0.2811(5)	0.25	3.1(4)
S	0.227(1)	0.1275(7)	0.1462(5)	1.6(3)

[a] $B(eq) = {}^4/_3[a^2\beta_{11} + b^2\beta_{22} + c^2\beta_{33} + ab(\cos\gamma)\beta_{12} + ac(\cos\beta)\beta_{13} + bc(\cos\alpha)\beta_{23}]$.

Results and Discussion

Synthesis. The syntheses and crystallization of **I–IV** were accomplished in A_2S_x (A = K or Rb) fluxes which were formed by the *in situ* reaction of A_2S and S in various ratios. The polysulfide melts serve as oxidation agents as well as reaction media which enhance the mobility of the reactants and help crystallization of the products. The mere result of quaternary phase formation in A_2S_x fluxes suggests that the reactions occur in a homogenized medium in which good mixing of Cu and Sn, and Au and Sn is achieved, probably through soluble sulfide precursor complexes. Such mixing is critical since Cu, Au and Sn alone can form stable ternary A/M/S compounds.[19]

(15) Smith, D. K.; Nichols, M. C.; Zolensky, M. JE. POWD10: A FORTRAN IV Program for Calculating X-ray Powder Diffraction Patterns; version 10, Pennsylvania State University.

(16) Sheldrick, G. M. In *Crystallographic Computing 3*; Sheldrick, G. M., Kruger, C., Goddard, R., Eds.; Oxford University Press: Oxford, U.K., 1985; pp 175–189.

(17) TEXSAN-TEXRAY Structure Analysis Package, Molecular Structure Corp., 1985.

(18) Walker, N.; Stuart, D. DIFABS: An Empirical Method for Correcting Diffraction Data for Absorption Effects. *Acta. Crystallogr.* **1983**, *A39*, 158–166.

(19) Kanatzidis, M. G. *Chem. Mater.* **1990**, *2*, 353–363.

Table III. Positional Parameters and Equivalent Isotropic Displacement Values (Å²)[a] for $Rb_2Cu_2Sn_2S_6$ with Estimated Standard Deviations in Parentheses

atom	x	y	z	B(eq)
Sn(1)	0.96959(7)	0.18745(7)	0.62863(5)	0.68(3)
Sn(2)	0.71978(7)	−0.06244(7)	0.62961(5)	0.68(3)
Rb(1)	1.3347(1)	0.0630(1)	0.58767(9)	1.56(5)
Rb(2)	0.9160(1)	0.1881(1)	0.41243(8)	1.45(5)
Cu(1)	1.0000	0.4322(2)	3/4	0.66(8)
Cu(2)	1.2478(1)	0.1933(3)	0.7499(1)	2.0(1)
Cu(3)	1.0000	−0.0643(2)	3/4	0.65(8)
S(1)	0.8660(3)	−0.1958(3)	0.6853(2)	0.8(1)
S(2)	0.6022(3)	0.0694(3)	0.6869(2)	0.9(1)
S(3)	1.1158(3)	0.0553(3)	0.6855(2)	1.0(1)
S(4)	0.8511(3)	0.3184(3)	0.6839(2)	1.0(1)
S(5)	1.0762(3)	0.3130(3)	0.5516(2)	1.6(1)
S(6)	0.8247(3)	0.0621(3)	0.5522(2)	1.2(1)

[a] $B(eq) = 4/3[a^2\beta_{11} + b^2\beta_{22} + c^2\beta_{33} + ab(\cos\gamma)\beta_{12} + ac(\cos\beta)\beta_{13} + bc(\cos\alpha)\beta_{23}]$.

Table IV. Positional Parameters and Equivalent Isotropic Displacement Values (Å²)[a] for $K_2Au_2SnS_4$ with Estimated Standard Deviations in Parentheses

atom	x	y	z	B(eq)
Au(1)	0.3306(1)	0.42189(9)	0.2678(1)	1.25(4)
Au(2)	0.7123(1)	0.8297(1)	0.4683(1)	1.25(4)
Sn	0.7245(2)	0.1941(2)	0.6254(2)	0.96(6)
K(1)	0.2549(6)	0.0792(6)	0.9707(7)	1.8(2)
K(2)	0.1860(7)	0.5796(6)	0.783(1)	2.8(3)
S(1)	0.5829(7)	0.2189(6)	0.2774(7)	1.3(2)
S(2)	0.0852(7)	0.6343(6)	0.240(1)	2.2(3)
S(3)	0.9194(7)	0.9375(6)	0.7084(8)	1.4(2)
S(4)	0.4964(7)	0.7443(6)	0.2133(8)	1.5(2)

[a] $B(eq) = 4/3[a^2\beta_{11} + b^2\beta_{22} + c^2\beta_{33} + ab(\cos\gamma)\beta_{12} + ac(\cos\beta)\beta_{13} + bc(\cos\alpha)\beta_{23}]$.

Table V. Positional Parameters and Equivalent Isotropic Displacement Values (Å²)[a] for $K_2Au_2Sn_2S_6$ with Estimated Standard Deviations in Parentheses

atom	x	y	z	B(eq)
Au	0.6889(1)	0	0.25	0.98(4)
Sn	0.5	0	0.41157(8)	0.66(6)
K(1)	0	0	0.0966(6)	1.9(2)
K(2)	0.5	0.5	0.25	4.3(6)
K(3)	0.5	0.5	0.0499	2.9(5)
S(1)	0.662(1)	0.149(1)	0.5	0.8(3)
S(2)	0.3227(7)	0.1772(8)	0.3453(2)	0.9(2)

[a] $B(eq) = 4/3[a^2\beta_{11} + b^2\beta_{22} + c^2\beta_{33} + ab(\cos\gamma)\beta_{12} + ac(\cos\beta)\beta_{13} + bc(\cos\alpha)\beta_{23}]$.

$Rb_2Cu_2SnS_4$ (I) was synthesized by heating Sn and Cu powder in a Rb_2S_5 flux at 400 °C. A Cu rich ratio (Sn:Cu = 1:4) was used to obtain I in pure form. The ratio of Sn:Cu = 1:2 gave $Rb_2Cu_2Sn_2S_6$ (II) while the ratio of 1:3 gave a mixture of I and II. The $Rb_2Cu_2Sn_2S_6$ phase dominates when Cu:Sn = 1:1. The Se analog was prepared in an analogous manner. All alkali-metal salts from Na^+ to Cs^+ form isomorphous sulfide phases. However, only K^+ and Rb^+ stabilized the selenide version.

$K_2Au_2SnS_4$ (III) was synthesized by heating Au and Sn powder in a ratio of 2:1 in a K_2S_5 flux at 350 °C, while $K_2Au_2Sn_2S_6$ (IV) was prepared by heating Au and Sn powder in a ratio of 1.5:1 in a K_2S_9 flux at 350 °C. IV, which contains $[Sn_2S_6]^{4-}$, fragmetns was synthesized under a sulfur-rich flux. This suggests that $[Sn_2S_6]^{4-}$, rather than $[SnS_4]^{4-}$, ions are favored in a more oxidizing sulfur-rich polysulfide flux. While this may seem counterintuitive, we point out that a sulfur-rich flux is less basic than a sulfide-rich (sulfur-poor) flux which breaks the $[Sn_2S_6]^{4-}$ dimers further into single $[SnS_4]^{4-}$ tetrahedra. It should be noted that the Sn:Au ratio (1:1.5) used in the reaction is not consistent with the chemical formula of $K_2Au_2Sn_2S_6$. Using the exact Sn:Au ratio (1:1) under the same reaction conditions gave a mixture of $K_2Au_2Sn_2S_6$ and reddish orange crystals of $K_2Sn_2S_8$.[10a] Only by increasing the Au content were we able to avoid the competitive side product. However, no ternary K/Au/S phases were observed, indicating that the excess Au forms soluble complexes which are removed during the isolation process.

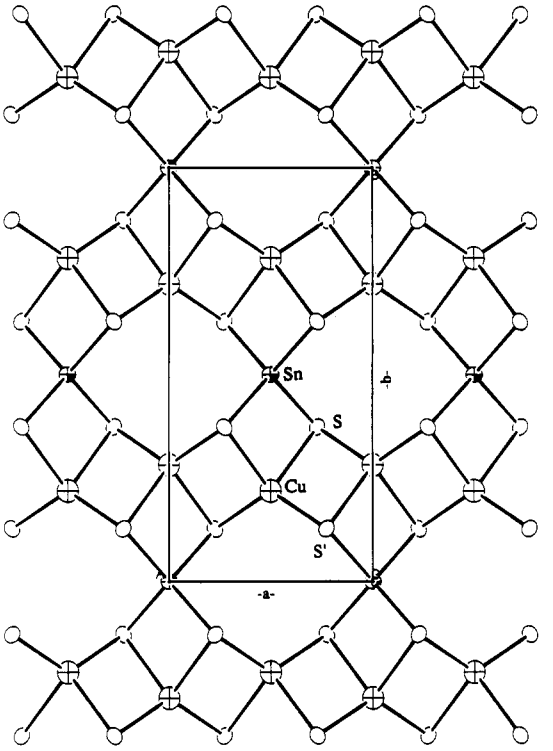

Figure 1. ORTEP representation and labeling scheme of the layered structure of $[Cu_2SnS_4]^{2-}$. View down the *c* axis.

Structure Description of $Rb_2Cu_2SnS_4$ (I). The $Rb_2Cu_2SnS_4$ is a layered compound. SnS_4 and CuS_4 tetrahedra in the ratio of 1:2 are the building blocks of the two-dimensional $[Cu_2SnS_4]_n^{2n-}$ framework, shown in Figure 1. The structure type of the two-dimensional anionic framework can be viewed as ordered defect anti-PbO[20] structure in which sulfur atoms occupy the lead sites, tin and copper atoms occupy the oxygen sites, but with one-half of tin atoms missing. We note that some ternary metal chalcogenides such as $Rb_2Mn_3S_4$, $Cs_2Mn_3S_4$, $Rb_2Co_3S_4$, $Cs_2Co_3S_4$, $Cs_2Zn_3S_4$, and $Rb_2Zn_3S_4$[21] are structurally related. In all these compounds the tetrahedral metal centers occupy three-fourths of the O sites in the PbO lattice. In the $[Cu_2SnS_4]_n^{2n-}$ framework, the CuS_4 tetrahedra share two opposite edges to form parallel infinite linear $[CuS_2]_n^{3n-}$ chains which are related to the $[FeS_2]^-$ chains in $KFeS_2$.[22] These chains are cross-linked by tetrahedral Sn^{4+} via sulfide ions in the $[CuS_2]_n^{3n-}$ chains. This arrangement leaves tetrahedral holes in the layers.

Selected bond distances and bond angles are given in Table VI. There are three mutually perpendicular crys-

(20) Boher, P.; Garnier, P.; Gavarri, J. R.; Hewat, A. W. *J. Solid State Chem.* **1985**, *57*, 343–350.
(21) (a) Bronger, W.; Böttcher, P. *Z. Anorg. Allg. Chem.* **1972**, *390*, 1–12. (b) Bronger, W.; Hendriks, U. *Rev. Chim. Miner.* **1980**, *17*, 555–560. (c) Bronger, W.; Müller, P. *J. Less-Common Met.* **1984**, *100*, 241–247.
(22) Boon, J. W.; MacGillavry, C. H. *Recl. Trav. Chim. Pays-Bas* **1942**, *61*, 910–917.

Table VI. Selected Bond Distances (Å) and Bond Angles (deg) of $Rb_2Cu_2SnS_4$ with Standard Deviations in Parentheses

Sn–S	2.390(8)	Rb–S	3.411(8)
Cu–S	2.583(8)	Rb–S	3.522(8)
Cu–S′	2.322(7)	Rb–S	3.462(8)
Cu–Cu	2.854(4)	Rb–S	3.417(8)
S–Sn–S	107.0(3)	S–Cu–S′	106.5(3)
S–Sn–S	104.9(4)	S′–Cu–S′	126.6(5)
S–Sn–S	116.7(3)	Sn–S–Cu	80.3(2)
S–Cu–S	94.5(4)	Sn–S′–Cu	104.5(3)
S–Cu–S′	109.1(2)	Cu–S–Cu	70.9(2)

tallographic 2-fold rotational axes passing through the Sn atoms. Therefore, all Sn–S distances are equal at 2.390(8) Å. Three pairs of S–Sn–S angles deviate from those in a perfect tetrahedron with 107.0(3)°, 104.9(4)°, and 116.7(3)°, respectively. There is a 2-fold axis passing through the CuS_4 tetrahedra which exhibit significant distortion from the ideal tetrahedron. The Cu···Cu distance is 2.854(4) Å. Two pairs of Cu–S distances are 2.582(8) and 2.322(7) Å. The significant difference of Cu–S bond distances is due to the difference in S–Cu–S bond angles. The S–Cu–S angle between the two shorter Cu–S bonds is a wide 126.6(5)°; the S–Cu–S angle between two longer Cu–S bonds is very narrow at 94.5(4)°. The other two pairs of S–Cu–S angles are 106.3(2)° and 109.1(2)°.

The rubidium cations are located between the anionic layers to balance the charge, as shown in Figure 2. The Rb^+ cations are sitting on a crystallographic mirror plane and are coordinated by eight sulfur atoms with an average Rb···S distance of 3.45(5) Å.

$SrCu_2SnS_4$,[11d] $BaCu_2SnS_4$,[11e] and $BaAg_2SnS_4$[11b] are related to **I** in their anionic stoichiometries but differ in structure. All of them are three-dimensional modified ZnS-type compounds formed by vertex-sharing CuS_4 and MS_4 (M = Cu or Ag) tetrahedra.

The two-dimensional anionic framework of **I** can be compared to that of KCu_2NbS_4,[23] which consists of edge-sharing NbS_4 and CuS_4 tetrahedra. Despite the similarity of their anionic formulae, the two frameworks differ in their arrangement of the MS_4 tetrathiometalate units. While the $[Cu_2SnS_4]^{2-}$ sheets are flat, those in KCu_2NbS_4 are highly corrugated. The conformational change from corrugated to flat is necessary to minimize the lattice energy because the number of cations is doubled in $Rb_2Cu_2SnS_4$. The defect anti-PbO structure of $Rb_2Cu_2SnS_4$ suggests that Cu^+ ion transport through the material might be possible via a hopping mechanism from the filled to the vacant sites.

Structure Description of $Rb_2Cu_2Sn_2S_6$ (II). $Rb_2Cu_2Sn_2S_6$ (**II**) has a two-dimensional structure containing corner-sharing tetrahedral CuS_4 and SnS_4 units, as shown in Figure 3. This is a derivative of the three-dimensional zinc blende adamantine type structure of the ternary parent compound Cu_2SnS_3.[24] The replacement of an alkali-metal ion for a Cu atom reduces the dimensionality of the Cu_2SnS_3 framework due to the interruption of covalent bonding throughout the structure. Each anionic slab, thus formed, contains three metal layers with a Cu layer sandwiched by two Sn layers in which one-half of the Sn sites are missing forming parallel grooves which run perpendicularly above and below the slabs. The Rb^+ cations are located inside the grooves as shown in Figure 4 and therefore are an integral part of the slabs. Thus, a true van der Waals gap exists between the $Rb_2Cu_2Sn_2S_6$ layers which must be stabilized partially by interlayer S···S interactions. Nevertheless, Rb···S interactions with adjacent layers also exist. This explains the material's thin-

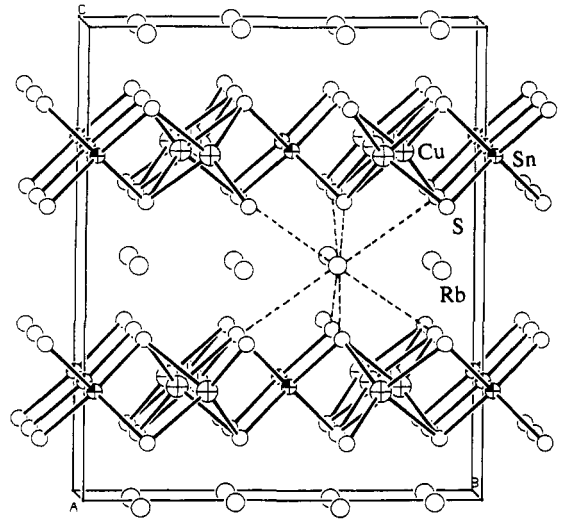

Figure 2. Structure of $Rb_2Cu_2SnS_4$ viewed parallel to the layers. A monolayer of rubidium cations are located between layers. Dash lines show the coordination environment of the Rb^+ cations.

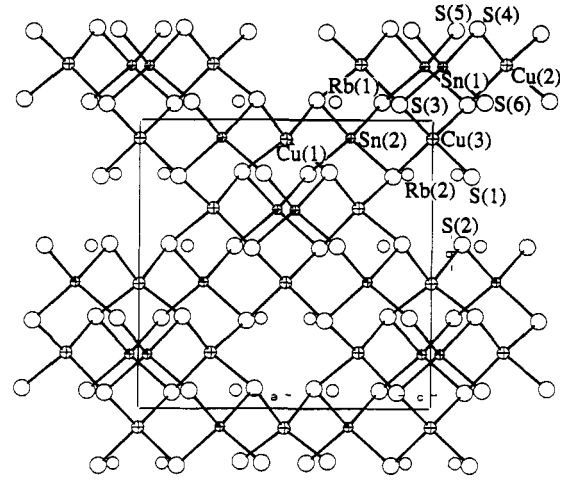

Figure 3. ORTEP representation and labeling scheme of the layered structure of $Rb_2Cu_2Sn_2S_6$. View down the *c* axis.

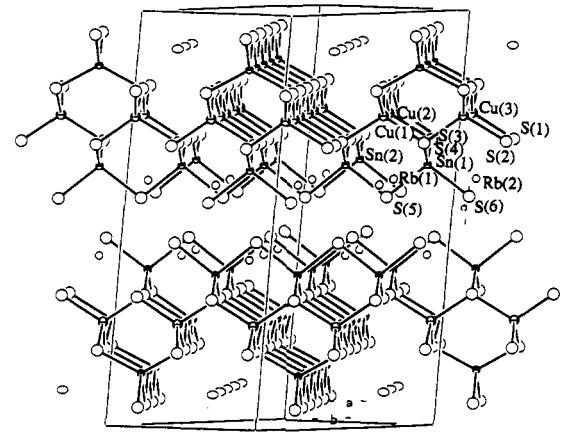

Figure 4. Structure of $Rb_2Cu_2Sn_2S_6$ viewed parallel to the layers.

(23) Keane, P. M.; Lu, Y.-J.; Ibers, J. A. *Acc. of Chem. Res.* **1991**, *24*, 223–229.

(24) Averkieva, G. K.; Vaipolin, A. A.; Goryunova, N. A. In *Some Ternary Compounds of the $A_2(I)B(IV)C_3(VI)$ Type and Solid Solutions Based on Them*, Soviet Research in New Semiconductor Materials, Nasledov, D. N., Ed.; Consultants Bureau: New York, 1965; pp 26–34.

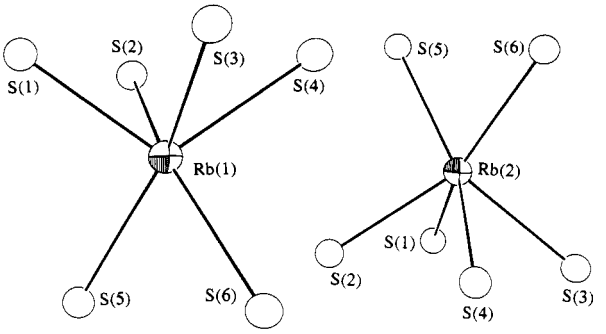

Figure 5. Coordination environment for Rb(1) and Rb(2). While S(1), S(2), S(3), and S(4) belong to the $[Cu_2Sn_2S_6]^{2-}$ slab which hosts the Rb^+ cations, S(5) and S(6) belong to another $[Cu_2Sn_2S_6]^{2-}$ slab.

layer crystal morphology and tendency to cleave easily into very thin mica-like sheets.

Two crystallographically distinct Rb^+ cations are situated within the anionic layers. Both are surrounded by six S atoms with an average Rb···S distance of 3.35(5) Å. Their coordination environments are similar, forming pseudo-C_{2v} symmetry as shown in Figure 5. The polyhedron of Rb^+, however, is best described as trigonal prismatic. Each Rb^+ cation is coordinated by four S atoms (S(1)–S(4)) from the $[Cu_2Sn_2S_6]^{2-}$ slab where it is situated and by two more S atoms (S(5), S(6)) from the adjacent layer.

Selected bond distances and angles of **II** are given in Table VII. The average Sn–S distance (2.42(8) Å) and the average Cu–S distance (2.35(2) Å) are normal. There are two types of sulfur atoms: S(1)–S(4) are triply bridging to two Cu atoms and one Sn atom while S(5)–S(6) are doubly bridging between two Sn atoms. The average Sn to S(1)–(4) distance (2.492(5) Å) are significantly longer than that of Sn to S(5)–S(6) distance (2.350(11) Å). Due to the stronger electronic repulsion between the shorter Sn–S bonds, the corresponding S–Sn–S bond angles are wider at 122.5(1)° and 122.3(1)°, whereas the S–Sn–S angle between two longer Sn–S bonds is smaller at 103.5(1)°. The remaining S–Sn–S angles and S–Cu–S angles do not show much deviation from that of an ideal tetrahedron.

Structure Description of $K_2Au_2SnS_4$ (III) and $K_2Au_2Sn_2S_6$ (IV). The one-dimensional anionic structure of **III** is constructed by SnS_4 tetrahedra and linear AuS_2 dumbbell units in the ratio of 1:2. Even though the stoichiometry of **III** is the same as that of **I**, the preferred linear coordination of Au^+ forces a dramatic structural change from that of **I**. The edges of two SnS_4 tetrahedra are connected by two Au^+ ions to form $Sn(SAuS)_2Sn$ eight-membered rings which extend in one dimension by sharing the Sn atoms at their two ends, as shown in Figure 6. These chains run along the crystallographic *b* axis and are parallel to one another, separated by charge balancing K^+ cations.

Selected bond distances and bond angles are given in Table VIII. The average Sn–S distance is 2.396(12) Å and the SnS_4 tetrahedra are slightly distorted with S–Sn–S angles ranging from 106.7(2)° to 111.9(2)° (average value = 109.4°) which are comparable to those in the discrete $[SnS_4]^{4-}$ ion.[10h-j] The average Au–S distance, 2.295(4) Å, is normal for linear AuS_2 fragments.[25] The average S–Au–S angle, 174.9(6)°, is close to 180°. The linear AuS_2 fragments in the $Sn(SAuS)_2Sn$ eight-membered rings are nearly parallel but the Au···Au distances are long at 3.929(2) and 4.014(3) Å. An interesting feature of the compounds is the presence of week intrachain Au···Au short contacts of 3.363(2) Å between two Au^+ ions in two adjacent $Sn(SAuS)_2Sn$ eight-membered rings as shown by the dashed lines in Figure 6. Interchain Au···Au short contacts were reported earlier, $KAuS_5$,[25,26] which contains two-coordinated Au^+ ions bridged with pentasulfides. No such contacts are observed in **III**. Two distinct K^+ cations are surrounded by seven and four S atoms, respectively. The average K···S distance is 3.31(13) Å. Regardless of the larger size of Au, the Au···K distances (3.546(5), 3.634(5), and 3.644(6) Å) are shorter than Sn···K distances (larger than 4 Å) and K···K distances (larger than 3.7 Å). Alkali metal···Au interactions were observed before.[27] The short K^+···Au distance suggests an attractive interaction of the d^{10} electron pairs on Au^+ ions and the positive charges on alkali-metal cations. The short contact may be accounted for by the relatively large electronegativity of Au, 2.4, which is remarkably close to those of Se(2.4) and Te(2.1).[28] An extreme case of alkali metal···Au interaction is found in

Table VII. Selected Bond Distances (Å) and Angles (deg) for $Rb_2Cu_2Sn_2S_6$ with Standard Deviations in Parentheses[a]

Sn(1)–S(3)	2.355(4)	Cu(3)–S(3)	2.353(4) × 2
Sn(1)–S(4)	2.334(4)	mean(Cu–S)	2.35(2)
Sn(1)–S(5)	2.498(4)	Rb(1)–S(1)	3.305(4)
Sn(1)–S(6)	2.490(4)	Rb(1)–S(2)	3.339(4)
Sn(2)–S(1)	2.354(4)	Rb(1)–S(3)	3.328(4)
Sn(2)–S(2)	2.356(4)	Rb(1)–S(4)	3.319(4)
Sn(2)–S(5)	2.494(4)	Rb(1)–S(5)	3.403(5)
Sn(2)–S(6)	2.487(4)	Rb(1)–S(6)	3.419(4)
mean(Sn–S)	2.42(8)	Rb(2)–S(1)	3.318(4)
Cu(1)–S(2)	2.365(4) × 2	Rb(2)–S(2)	3.337(4)
Cu(1)–S(4)	2.339(4) × 2	Rb(2)–S(3)	3.329(4)
Cu(2)–S(1)	2.318(4)	Rb(2)–S(4)	3.308(4)
Cu(2)–S(2)	2.382(4)	Rb(2)–S(5)	3.412(4)
Cu(2)–S(3)	2.372(4)	Rb(2)–S(6)	3.430(4)
Cu(2)–S(4)	2.300(5)	mean(Rb–S)	3.35(5)
Cu(3)–S(1)	2.342(4) × 2		
S(3)–Sn(1)–S(4)	122.5(1)	S(2)–Cu(2)–S(4)	112.2(1)
S(3)–Sn(1)–S(5)	107.5(1)	S(3)–Cu(2)–S(4)	113.7(1)
S(3)–Sn(1)–S(6)	107.5(1)	S(1)–Cu(3)–S(1)	103.5(2)
S(4)–Sn(1)–S(5)	107.5(1)	S(1)–Cu(3)–S(3)	112.5(1) × 2
S(4)–Sn(1)–S(6)	106.8(1)	S(1)–Cu(3)–S(3)	108.1(1) × 2
S(5)–Sn(1)–S(6)	103.5(1)	S(3)–Cu(3)–S(3)	111.9(2)
S(1)–Sn(2)–S(2)	122.3(1)	Sn(2)–S(1)–Cu(2)	101.5(1)
S(1)–Sn(2)–S(5)	107.2(1)	Sn(2)–S(1)–Cu(3)	102.8(1)
S(1)–Sn(2)–S(6)	107.5(1)	Cu(2)–S(1)–Cu(3)	111.7(2)
S(2)–Sn(2)–S(5)	108.0(1)	Sn(2)–S(2)–Cu(1)	102.0(1)
S(2)–Sn(2)–S(6)	107.8(1)	Sn(2)–S(2)–Cu(2)	103.4(1)
S(5)–Sn(2)–S(6)	102.2(1)	Cu(1)–S(2)–Cu(2)	114.9(2)
S(2)–Cu(1)–S(2)	100.5(2)	Sn(1)–S(3)–Cu(2)	101.6(1)
S(2)–Cu(1)–S(4)	112.4(1) × 2	Sn(1)–S(3)–Cu(3)	103.4(1)
S(2)–Cu(1)–S(4)	107.7(1) × 2	Cu(2)–S(3)–Cu(3)	113.0(2)
S(4)–Cu(1)–S(4)	115.2(2)	Sn(1)–S(4)–Cu(1)	102.2(1)
S(1)–Cu(2)–S(2)	101.8(1)	Sn(1)–S(4)–Cu(2)	104.5(2)
S(1)–Cu(2)–S(3)	112.1(1)	Cu(1)–S(4)–Cu(2)	109.7(2)
S(1)–Cu(2)–S(4)	111.2(2)	Sn(1)–S(5)–Sn(2)	102.7(2)
S(2)–Cu(2)–S(3)	105.0(2)	Sn(1)–S(6)–Sn(2)	103.1(1)

[a] The mean bond lengths are calculated by the equation $l = (\sum_n l_n)/n$. The estimated standard deviations in the mean bond lengths are calculated by the equation: $\sigma_l = \{\sum_n (l_n - l)^2/(n-1)\}^{1/2}$, where l_n is the length of the *n*th bond, *l* the mean length, and *n* the number of the bonds.

(25) Park, Y.; Kanatzidis, M. G. *Angew. Chem., Int. Ed. Engl.* **1990**, *29*, 914–915.

(26) Whangbo, M.-H. in *Crystal Chemistry and Properties of Materials with Quasi-One-Dimensional Structures*; Rouxel, J., Ed.; D. Reidel: Dordrecht, 1986; pp 27–85.

(27) (a) Haushalter, R. C. *Angew. Chem., Int. Ed. Engl.* **1985**, *24*, 432–433. (b) Huang, S.-P.; Kanatzidis, M. G. *Angew. Chem., Int. Ed. Engl.* **1992**, *31*, 787–789.

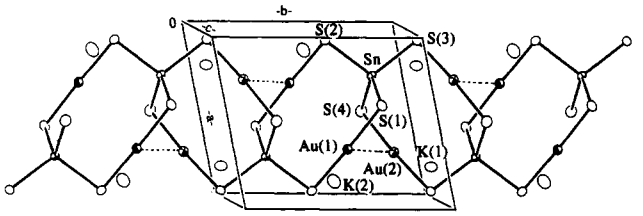

Figure 6. ORTEP representation and labeling scheme of a single chain of $K_2Au_2SnS_4$. Au···Au short contacts are shown by dashed lines.

Table VIII. Selected Bond Distances (Å) and Bond Angles (deg) of $K_2Au_2SnS_4$ with Standard Deviations in Parentheses[a]

Au(1)-S(1)	2.297(5)	Sn-S(1)	2.384(5)q
Au(1)-S(2)	2.290(6)	Sn-S(2)	2.410(5)
Au(2)-S(3)	2.300(5)	Sn-S(3)	2.398(5)
Au(2)-S(4)	2.293(5)	Sn-S(4)	2.401(6)
mean(Au-S)	2.295(4)	mean(Sn-S)	2.398(11)
Au(1)-Au(2)	3.363(2)	K(1)-S(1)	3.264(7)
Au(2)-Au(2)	4.015(3)	K(1)-S(2)	3.224(8)
Au(1)-Au(1)	3.929(2)	K(1)-S(3)	3.248(7)
Au(1)-K(1)	3.634(5)	K(1)-S(3)	3.209(8)
Au(1)-K(2)	3.644(6)	K(1)-S(4)	3.401(8)
Au(2)-K(2)	3.865(6)	K(1)-S(4)	3.642(7)
Au(2)-K(2)	3.914(6)	K(2)-S(1)	3.186(8)
Au(2)-K(1)	3.546(5)	K(2)-S(2)	3.332(8)
Au(2)-K(1)	3.999(5)	K(2)-S(3)	3.303(7)
mean(Au-S)	3.77(18)	K(2)-S(4)	3.269(8)
K(1)-S(1)	3.283(7)	mean(K-S)	3.31(12)
S(1)-Sn-S(2)	110.5(2)	S(1)-Au(1)-S(2)	175.1(2)
S(1)-Sn-S(3)	110.9(2)	S(3)-Au(2)-S(4)	174.6(2)
S(1)-Sn-S(4)	111.9(2)	Au(2)-S(3)-Sn	92.0(2)
S(2)-Sn-S(3)	106.7(2)	Au(1)-S(1)-Sn	99.0(2)
S(2)-Sn-S(4)	107.4(2)	Au(2)-S(4)-Sn	95.1(2)
S(3)-Sn-S(4)	109.2(2)	Au(1)-S(2)-Sn	92.8(2)

[a] The mean bond lengths are calculated by the equation $l = (\sum_n l_n)/n$. The estimated standard deviations in the mean bond lengths are calculated by the equation: $\sigma l = \{\sum_n (l_n - l)^2/(n-1)\}^{1/2}$, where l_n is the length of the nth bond, l the mean length, and n the number of the bonds.

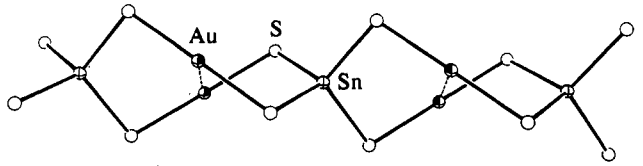

Figure 7. ORTEP representation of the anionic structure of $BaAu_2SnS_4$ adapted from ref 11a.

KAu_5[29] in which K···Au distances range from 3.27 to 3.61 Å.

We note that in $BaAu_2SnS_4$ (V)[11a] the $[Au_2SnS_4]^{2-}$ chains contain the same building blocks as in **III** but adopt a different conformation, as shown in Figure 7. In $BaAu_2SnS_4$, all Sn atoms lie in a straight line, while in **III** the Sn-Sn vectors in the $Sn(SAuS)_2Sn$ eight-membered rings proceed in a zigzag fashion with the angle between two Sn-Sn vectors at 107.46(6)°. The conformational change is clearly due to packing effects and can be explained by the difference in size and number of the counterions between **III** and **V**. Zigzag chains are better able to accommodate a double row of K^+ cations. The straight chains of the Ba^{2+} salt provide enough space for a single row of Ba^{2+} cations. This is illustrated by comparing parts A and B of Figure 8. The structures of $K_2Au_2SnS_4$ and

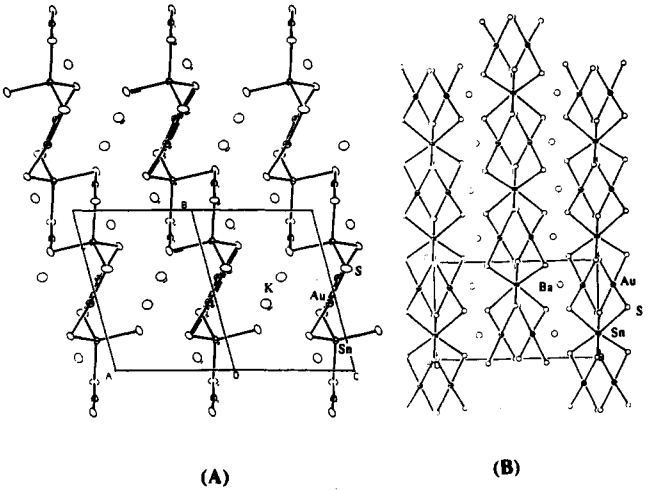

Figure 8. Comparison between the unit cells of (A) $K_2Au_2SnS_4$ viewed down the ⟨101⟩ axis. (B) $BaAu_2SnS_4$ viewed down the ⟨010⟩ axis.

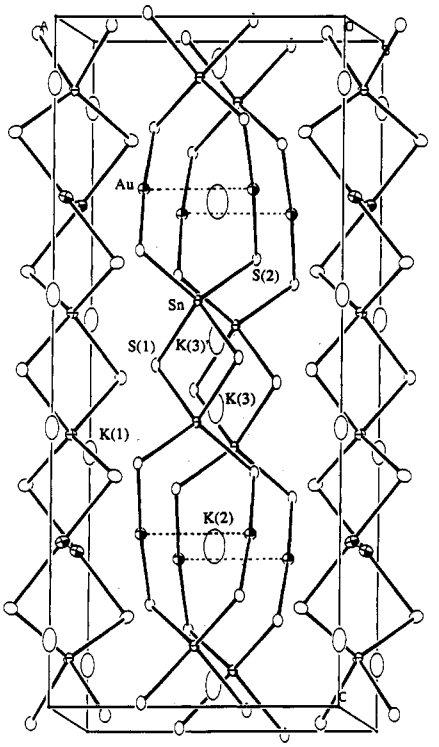

Figure 9. ORTEP representation and labeling scheme of $K_2Au_2Sn_2S_6$. Au···Au short contacts are shown by dashed lines.

$BaAu_2SnS_4$ are also closely related to those of $K_2Hg_3S_4$, $K_2Hg_3Se_4$, and $Cs_2Hg_3Se_4$[30] (which can be written as $A_2Hg_2Hg'Q_4$ (A = alkali metal; Q = S, Se) for a more obvious comparison). These compounds feature straight $[Hg_3Q_4]^{2-}$ chains in which $[HgS_4]^{6-}$ tetrahedra are connected via linear Hg^{2+} centers.

The $[Au_2Sn_2S_6]^{2-}$ fragment in **IV** is also one-dimensional, featuring edge-sharing bitetrahedral $[Sn_2S_6]$ units connected by linear Au^+ atoms to form infinite chains. The chains are fully extended by comparison to the zigzag motif exhibited in **III**. The unit cell of $K_2Au_2Sn_2S_6$ is shown in Figure 9. The structure of **IV** is also related to that of fully extended $BaAu_2SnS_4$. **IV** contains longer

(28) Greenwood, N. N.; Earnshaw, A. *Chemistry Of The Elements*; Pergamon Press: New York, 1986, Ltd.

(29) Raub, C.; Compton, V. *Z. Anorg. Allg. Chem.* **1964**, *332*, 5–11.

(30) (a) Kanatzidis, M. G.; Park, Y. *Chem. Mater.* **1990**, *2*, 99–101. (b) Kanatzidis, M. G.; Park, Y. *Chem. Mater.* **1990**, *2*, 353–363. (c) Park, Y. Dissertation, Michigan State University, 1992.

Table IX. Selected Bond Distances (Å) and Angles (deg) for $K_2Au_2Sn_2S_6$ with Standard Deviations in Parentheses[a]

Au-Au	3.010(2)	K(1)-S(1)	3.477(9)
Au-S(2)	2.313(5)	K(1)-S(2)	3.138(7)
Sn-S(1)	2.443(7)	K(2)-S(2)	3.459(6)
Sn-S(2)	2.368(6)	K(3)-S(1)	3.226(9)
mean(Sn-S)	2.41(5)	K(3)-S(2)	3.559(6)
Au-K(1)	3.850(8)	mean(K-S)	3.39(16)
Au-Au-S(2)	87.7(1)	S(2)-Au-S(2)	175.4(3)
Au-Au-S(2)	87.7(1)	S(1)-Sn-S(2)	110.3(2)
S(1)-Sn-S(1)	91.9(3)	S(1)-Sn-S(2)	113.5(2)
S(1)-Sn-S(2)	113.5(2)	S(2)-Sn-S(2)	115.0(2)
S(1)-Sn-S(2)	110.3(2)	Sn-S(1)-Sn	88.1(3)

[a] The mean bond lengths are calculated by the equation $l = \{\sum_n (l_n - l)^2/(n-1)\}^{1/2}$, where l_n is the length of the nth bond, l the mean length, and n the number of the bonds.

Table X. Summary of the Optical Bandgaps (eV) for $Rb_2Cu_2SnS_4$, $A_2Cu_2Sn_2S_6$ (A = K, Rb), $A_2Cu_2Sn_2Se_6$ (A = K, Rb), $K_2Au_2SnS_4$, and $K_2Au_2Sn_26$

compound	E_g (eV)	compound	E_g (eV)
$Rb_2Cu_2SnS_4$	2.08	$K_2Cu_2Sn_2Se_6$	1.04
$K_2Cu_2Sn_2S_6$	1.47	$R_2Cu_2Sn_2Se_6$	1.04
$Rb_2Cu_2Sn_2S_6$	1.44	$K_2Au_2SnS_4$	2.75
		$K_2Au_2Sn_2S_6$	2.30

$[Sn_2S_6]^{4-}$ units so that the chains can accommodate 1 more equivalent of K^+ cations. The $[Au_2Sn_2S_6]^{2-}$ chains lie parallel to the crystallographic c axis and are separated by potassium cations.

Selected bond distances and angles for **IV** are given in Table IX. The average Sn-S distances is 2.41(4) Å and the S-Sn-S angles range from 91.9(3)° to 115.0(2)°, which are comparable to those in discrete $[Sn_2S_6]^{4-}$ ions.[11g] The Au-S distances and S-Au-S angles are comparable to those in **III** at 2.313(5) Å and 175.4(3)°. There is also a Au···Au short contact at 3.010(2) Å. The Au···Au short contact occurs inside the $Sn(SAuS)_2Sn$ eight-membered ring in contrast with **III** in which inter-ring Au···Au are found. The Au···Au short contacts are classical d^{10}–d^{10} interactions[31] which were also observed in $BaAu_2SnS_4$ and $KAuS_5$. The two linear AuS_2 fragments in the $Sn(SAuS)_2Sn$ eight-membered rings are not parallel but form a S-Au···Au-S dihedral angle of 75.3°.

There are three distinct potassium cations. K(1) and K(2) are coordinated by 8 and 10 S atoms, respectively, while K(3) is found to be disordered evenly between (0.5, 0.5, 0.049) and (0.5, 0.5, −0.049). At either site, K(3) is coordinated by eight S atoms. The average K···S distance is 3.39(16) Å. The K···Au distances at 3.850(8) Å are longer than those in **III**. We note that the K^+ cations are surrounded by more S atoms in **IV**, and, as a result, a fewer number of K···Au interactions are observed.

Although gold and copper belong to the same group in the periodic table, they behave quite differently in their coordination modes. Tetrahedral coordination is the most common for Cu^+ chalcogenides although three- and two-coordinated Cu^+ are known. Au^+ prefers linear coordination because of the very large (4.63 eV) 6s–6p energy separation which makes mixing and hybridization of these orbitals more difficult.[32] The less common Au^{3+} square-planar centers were formed in the ternary $AAuSe_2$ (A = Na, K), Na_3AuSe_8 and K_3AuSe_{13}[20,25,30c] systems and appear to be more stable in a selenide environment rather than sulfide. Extension of the studies reported here into the Se_x^{2-} fluxes may also stabilize Au^{3+} centers which, in conjunction with Sn and alkali metals, should form different structures than those described here.

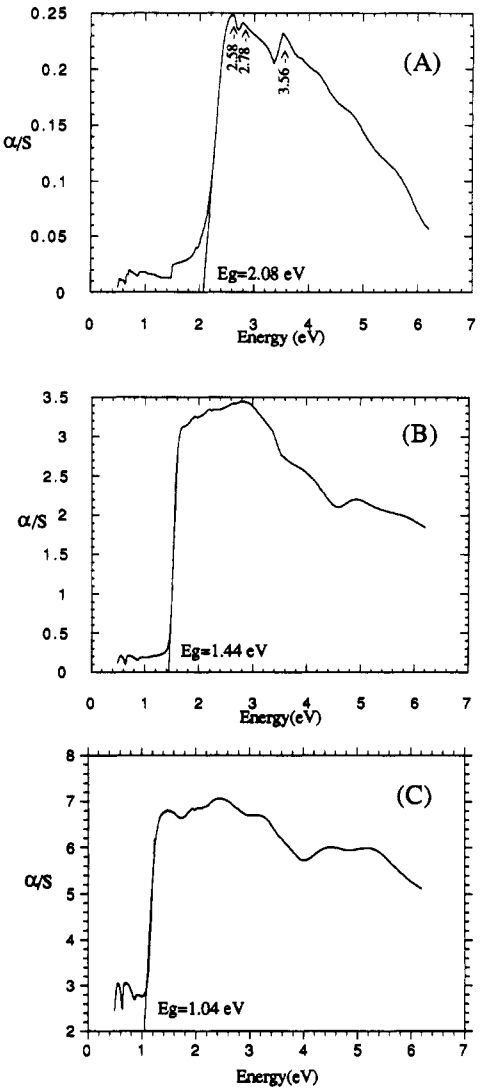

Figure 10. Optical absorption spectra of (A) $Rb_2Cu_2SnS_4$, (B) $Rb_2Cu_2SnS_6$, and (C) $K_2Cu_2Sn_2Se_6$.

Optical Spectroscopy. The UV-vis-near-IR spectra of all compounds reported here exhibit steep absorption edges from which optical band gaps can be unequivocally derived. $(\alpha h\nu)^2$ vs E plots appear quite linear suggesting the band gaps are direct in character. Table X summarizes the results. Typical absorption spectra are shown in Figures 10 and 11. The bandgap values are consistent with the colors of the samples. These results suggests that all compounds are semiconductors as predicted by the electron precise nature of their chemical formulas. The spectrum of $Rb_2Cu_2SnS_4$ also reveals other electronic transitions at higher energy (2.58, 2.78, and 3.56 eV) above the absorption edge. The selenide analogs $K_2Cu_2Sn_2Se_6$ and $Rb_2Cu_2Sn_2Se_6$ absorb at lower energy, as expected,

(31) (a) Jason, M. *Angew. Chem., Int. Ed. Engl.* **1987**, *26*, 1098–1111. (b) Scherbaum, F.; Huber, B.; Müller, G.; Schmidbauer, H. *Angew. Chem., Int. Ed. Engl.* **1988**, *27*, 1542–1544. (c) Kahn, M. N. I.; King, C.; Heinrich, D. D.; Fackler, J. P., Jr.; Porter, L. C. *Inorg. Chem.* **1988**, *28*, 2150–2154. (d) Fackler, J. P., Jr.; Porter, L. C. *J. Am. Chem. Soc.* **1986**, *108*, 2750–2751. (e) Merz, K. M., Jr.; Hoffmann, R. *Inorg. Chem.* **1988**, *27*, 2120–2127. (f) Jansen, M. *Angew. Chem., Int. Ed. Engl.* **1984**, *23*, 1098–1109. (g) Mehrotra, R.; Hoffmann, R. *Inorg. Chem.* **1978**, *17*, 2187–2189. (h) Pathaneni, S. S.; Desiraju, G. R. *J. Chem. Soc., Daltan Trans.* **1993**, 319–322.

(32) Fergusson, J. E. In *Stereochemistry and Bonding in Inorganic Chemistry*; Prentice-Hall: New York, 1974; pp 194–196.

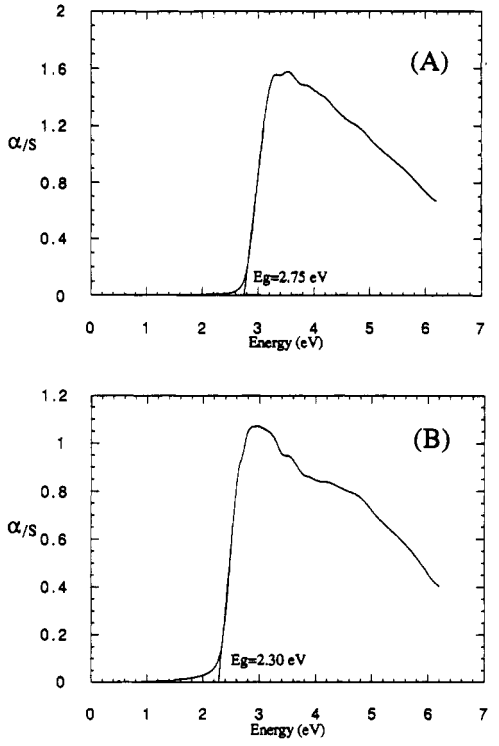

Figure 11. Optical absorption spectra of (A) $K_2Au_2SnS_4$ and (B) $K_2Au_2Sn_2S_6$.

giving bandgaps in the neighborhood of 1.04 eV; see Figure 10C. The bandgaps of $A_2Cu_2Sn_2S_6$ and $A_2Cu_2Sn_2Se_6$ are relatively low and comparable to those of the structurally related chalcopyrites, $CuInS_2$ (1.55 eV) and $CuInSe_2$ (1.0 eV). These values suggest that these compounds are suitable for efficient absorption of most of the solar radiation making them potential candidates for solar cell applications. In $CuInQ_2$, the optical bandgap transition originates from a valence band, composed of orbitals hybridized Cu(3d)/Q(3 or 4p) to a Cu(4s) conduction band.[33] A similar assignment is proposed for $A_2Cu_2Sn_2Q_6$. The small bandgaps exhibited by $A_2Cu_2Sn_2Q_6$ are also comparable to that of CdTe (1.5 eV), GaAs (1.4 eV), and Si (1.1 eV) which, together with $CuInQ_2$, are highly efficient photovoltaic materials.[34]

Conclusion

The results reported here show that the $[SnS_4]^{4-}$ and $[Sn_2S_6]^{4-}$ anions are excellent building blocks which can be linked with other metal ions to form various extended quaternary structures. The ability of the $[SnS_4]^{4-}$ and $[Sn_2S_6]^{4-}$ ligands to coordinate to M^{n+} ions in solid-state structures may parallel or exceed that of the versatile $[MoS_4]^{2-}$ exhibited in discrete complexes, and thus it points to a promising new synthetic avenue in which tetrathiometalates play a central role. Alkali polysulfide fluxes are not only convenient but perhaps superior *in situ* sources for these anions.

Acknowledgment. Support from the National Science Foundation (DMR-9202428) and the Beckman Foundation is greatly appreciated. M.G.K. is an A.P. Sloan Foundation Fellow 1991–93 and a Camille and Henry Dreyfus Teacher Scholar 1993–95. The work made use of the SEM facilities of the Center of Electron Optics at Michigan State University.

Supplementary Material Available: Tables of calculated and observed X-ray powder diffraction patterns and anisotropic thermal parameters of all atoms (6 pages); a listing of calculated and observed ($10F_o/10F_c$) structure factors (32 pages). Ordering information is given on any current masthead page.

(33) (a) Shay, J. L.; Tell, B.; Kasper, H. M. *Phys. Rev. Lett.* **1972**, *29*, 1162–1164. (b) Shay, J. L.; Kasper, H. M.; Schiavone, L. M. *Phys. Rev.* **1972**, *B5*, 5003–5005. (c) Tell, B.; Kasper, H. M. *Phys. Rev.* **1971**, *B4*, 2463–2471.

(34) (a) Zweibel, K.; Mitchell, R. In *$CuInSe_2$ and CdTe: Scale-Up for Manufacturing*; SERI Publication, prepared for US DOE under Contract No. DE-AC02-83CH10093, 1989. (b) Champness, C. H. *Phosphorus Sulfur* **1988**, *38*, 385–397.